

A Switched Systems Approach to Path Following With Intermittent State Feedback

Hsi-Yuan Chen , Zachary I. Bell , Patryk Deptula , and Warren E. Dixon , *Fellow, IEEE*

Abstract—Autonomous agents are often tasked with operating in an area where feedback is unavailable. Inspired by such applications, this paper develops a novel switched system-based control method for uncertain nonlinear systems with temporary loss-of-state feedback. To compensate for intermittent feedback, an observer is used while state feedback is available to reduce the estimation error, and a predictor is utilized to propagate the estimates while state feedback is unavailable. Based on the resulting subsystems, maximum and minimum dwell time conditions are developed via a Lyapunov-based switched systems analysis to relax the constraint of maintaining constant feedback. Using the dwell time conditions, a switching trajectory is developed to enter and exit the feedback denied region in a manner that ensures that the overall switched system remains stable. A scheme for designing a switching trajectory with a smooth transition function is provided. Simulation and experimental results are presented to demonstrate the performance of control design.

Index Terms—Dwell time conditions, intermittent state feedback, observer, predictor, switched systems theory.

I. INTRODUCTION

AQUIREING state feedback is at the core of ensuring stability in control designs. However, factors such as the task definition, operating environment, or sensor modality can result in temporary loss of feedback. For example, agents may be required to limit communication during predefined time frames or when traversing through certain regions. Motivated by such factors, various path planning and control methods have been developed that seek to ensure uninterrupted feedback (cf., [1]–[12]). Such results inherently constrain the trajectory or behavior of a system. For instance, visual servoing applications for nonholonomic systems can result in limited, sharp-angled, or nonsmooth trajectories to keep a target in the camera field of view (FOV) as illustrated in results such as [13]–[15]. Rather than trying to constrain the system to ensure continuous

feedback availability, the approach in this paper leverages switched systems methods to achieve an objective despite intermittent feedback. Some applications where this approach is useful include underwater operations that require vehicles to resurface to acquire GPS, navigation within urban canyons where GPS is occluded, and exploration of areas where absolute positioning systems have not been established (cf., [16]–[18]).

Solutions to relaxing the constant feedback constraint have been investigated. For example, methods to relax the requirement of keeping landmarks in the FOV have been developed in results such as [19] and [20]. In [19], multiple landmarks are linked together by a daisy-chaining approach where new landmarks are mapped onto the initial world frame and are used to provide state feedback when initial landmarks leave the FOV. Similar concepts were adopted in [20], where a wheeled mobile robot is allowed to navigate around a landmark without constantly keeping it in the FOV by relating feature points in the background to the landmark and thus provide state feedback. Although the objective to eliminate the requirement of constant visual on the landmark is achieved, state feedback is assumed to be available during periods when the landmark is outside the FOV. Such daisy-chaining approaches provide state feedback in an ideal scenario, but the accuracy of the feedback may degrade or even diverge in the presence of measurement noise and disturbances in the dynamics.

Conventional approaches to the simultaneous localization and mapping (SLAM) problem, such as the works in [21]–[23], use relationships between features or landmarks to estimate the pose (i.e., position and orientation) of the sensor, usually a monocular camera, and simultaneously determine the position of landmarks with respect to the world frame. Typically, a feature-rich environment with sufficient measurements are required for SLAM methods to provide state estimation. However, a well-known drawback with SLAM algorithms is that without proper loop closures the estimates will drift over time due to the accumulation of measurement noise (cf., [24], [25]). In this paper, a state estimate dynamic model propagates the state estimate when feedback is not available, and no additional feedback information is required. In SLAM applications, the feedback regions defined in this paper can be represented as features or landmarks with known absolute position. Hence, stability can be achieved by closing the loop with respect to these known features or landmarks, and sufficient conditions may be derived via a Lyapunov-based analysis to ensure that the loop closures are achieved before the state estimates degrade beyond a desired threshold.

Manuscript received November 25, 2018; accepted January 28, 2019. Date of publication March 20, 2019; date of current version May 31, 2019. This paper was recommended for publication by Associate Editor Andreas Mueller upon evaluation of the reviewers' comments. This work was supported in part by Air Force Office of Scientific Research (AFOSR) under Award FA9550-18-1-0109 and in part by Naval Engineering Education Consortium (NEEC) under Award N00174-18-1-0003. (*Corresponding author: Hsi-Yuan Chen.*)

The authors are with the Department of Mechanical and Aerospace Engineering, University of Florida, Gainesville, FL 32611 USA (e-mail: hychen@ufl.edu; bellz121@ufl.edu; pdeptula@ufl.edu; wdixon@ufl.edu).

This paper has supplementary downloadable multimedia material available at <http://ieeexplore.ieee.org> provided by the authors. This includes a video, which shows a recording of the experiment with the motion of the quadcopter and the switching trajectory projected on the floor. This material is 30.0 MB in size.

Color versions of one or more of the figures in this paper are available online at <http://ieeexplore.ieee.org>.

Digital Object Identifier 10.1109/TRO.2019.2899269

Stability of systems that experience random state feedback has been analyzed in previous literature. Typically, the intermittent loss of measurement is modeled as a random Bernoulli process with a known probability. Resulting trajectories are then analyzed in a probabilistic sense, where the expected value of the estimation error is shown to converge asymptotically, compared to the result in this paper which examines the behavior of the actual tracking and estimation errors.

The networked control systems community has also examined systems with temporarily unavailable measurements. Results such as [26]–[29] rely on a decision maker that is independent of the estimator or controller to determine when to broadcast sensor information. The objective in these results is to minimize the cost of network bandwidth by reducing the frequency of data transmission. In [30]–[32], data loss is modeled as random missing outputs and noisy measurements. In each case, state estimates are propagated by a model of the controlled system during the periods when transmission is missing. On the contrary, the availability of sensor information in this paper is determined by the region in which the actual states are located, which introduces a unique constraint of state-based feedback availability (i.e., even if a decision maker indicates that state information should be made available, the agent has to leave its current objective to return to a region where it can obtain state information.) Therefore, sensor information is only available when the states are inside a feedback region.

It is well-known that slow switching between stable subsystems may result in instability as explained in [33]. For slow switching between stable subsystems, the underlying strategy for proving stability involves developing switching conditions to ensure the overall system is stable. If a common Lyapunov function exists for all subsystems such that the time derivative of the Lyapunov function is upper bounded by a common negative definite function, the overall system is proven to be stable in [33]. For cases where a common Lyapunov function cannot be determined, multiple subsystem-specific Lyapunov functions are used. In general, the overall Lyapunov function is discontinuous and jumps may occur at switching interfaces. Therefore, the stability of such a system is achieved by placing switching conditions on the subsystems to enforce a decrease in the subsystem-specific Lyapunov functions between each successive activation of the respective subsystems. Typically, these requirements manifest as (average) dwell time conditions which specifies the duration for which each subsystem must remain active, as described in [33].

When a subset of the subsystems is unstable, a layer of complication is introduced into the analysis. A stability analysis is provided in [34] for switched systems with stable and unstable linear time-invariant subsystems, where an average dwell time condition is developed. Similarly, in [35], Müller and Liberzon developed dwell time conditions for nonlinear switched systems with exponentially stable and unstable subsystems. However, dwell time conditions typically require the stable subsystems to be activated longer than the unstable subsystems, as indicated in [34]. In [36], Parikh *et al.* developed an observer to estimate the depths of feature points in an image from a monocular camera and use a predictor to propagate the state estimates when the features are occluded or outside the FOV. Based on the error system

formulation, the subsystem for the observer is stable, while the subsystem for the predictor is unstable. An average dwell time condition is developed to ensure the stability of the switched system. However, the focus of [36] is the estimation of feature depths and therefore, not on achieving a control objective when feedback is unavailable.

The development in this paper aims to achieve a path-following objective despite intermittent loss of feedback. The novelty of this result is guaranteeing the stability of following a path which lies outside a region with feedback while maximizing the amount of time the agent spends in the feedback-denied environment. Switched systems methods are used to develop a state estimator and predictor when state feedback is available or not, respectively. Since switching occurs between a stable subsystem when feedback is available and an unstable subsystem when feedback is not available, dwell time conditions are developed that determine the minimum time that the agent must be in the feedback region versus the maximum time the agent can be in the feedback-denied region. Using these dwell time conditions, a switching trajectory is designed based on the dwell time conditions that leads the agent in and out of the feedback-denied region so that the overall system remains stable. The most similar result to this paper is in [37], which includes state prediction and control for a nonholonomic system moving around an obstacle. The goal in [37] is to regulate a nonholonomic vehicle to a set point in the presence of intermittent feedback. However, the difficulty of path following in the current paper arises when the system is outside the feedback region.

This paper is organized as follows. In Section II, the system model is introduced. In Section III, the tracking and estimation objective is given and the respective error systems are defined. Based on the error dynamics, a Lyapunov-based stability analysis for the resulting switched system is performed in Section V to develop the dwell time conditions and to show the stability of the overall system. In Section VI, a strategy for designing a switching trajectory is presented. A simulation is provided in Section VII and an experiment is provided in Section VIII to demonstrate the performance of the approach.

II. SYSTEM MODEL

Consider a dynamic system subject to an exogenous disturbance as

$$\dot{x}(t) = f(x(t), t) + v(t) + d(t) \quad (1)$$

where $x(t)$, $\dot{x}(t) \in \mathbb{R}^n$ denote a generalized state and its time derivative, $f : \mathbb{R}^n \times \mathbb{R} \rightarrow \mathbb{R}^n$ denotes the locally Lipschitz drift dynamics, $v(t) \in \mathbb{R}^n$ is the control input, and $d(t) \in \mathbb{R}^n$ is the exogenous disturbance where $n \in \mathbb{N}$ and $t \in \mathbb{R}_{\geq 0}$.

Assumption 1: The Euclidean norm of the exogenous disturbance $d(t)$ is bounded by $\|d(t)\| \leq \bar{d} \in \mathbb{R}_{\geq 0}$.

III. STATE ESTIMATE AND CONTROL OBJECTIVE

In this paper, the overall objective is to achieve path following under intermittent loss of feedback. Specifically, a known feedback region is denoted as a closed set $\mathcal{F} \subset \mathbb{R}^n$, where the complement region where feedback is unavailable is denoted by

\mathcal{F}^c . That is, feedback is available when $x(t) \in \mathcal{F}$ and unavailable when $x(t) \in \mathcal{F}^c$.

A desired path is denoted as $x_d \subset \mathcal{F}^c$. It is clear that state feedback is unavailable while attempting to follow x_d , and hence the system must return to the feedback region \mathcal{F} intermittently to maintain stability. Therefore, a switching trajectory, denoted by $\bar{x}_d(t) \in \mathbb{R}^n$, is designed to overlay x_d as much as possible while adhering to the subsequently developed dwell time constraints. To quantify the ability of the controller to track the switching trajectory, the tracking error $e(t) \in \mathbb{R}^n$ is defined as

$$e(t) \triangleq e_1(t) + e_2(t) \quad (2)$$

where the estimate tracking error $e_1(t) \in \mathbb{R}^n$ is defined as

$$e_1(t) \triangleq \hat{x}(t) - \bar{x}_d(t) \quad (3)$$

and the state estimation error $e_2(t) \in \mathbb{R}^n$ is defined as

$$e_2(t) \triangleq x(t) - \hat{x}(t) \quad (4)$$

where $\hat{x}(t) \in \mathbb{R}^n$ is the state estimate.

Based on (3) and (4), the control objective is to ensure that $e_1(t)$ and $e_2(t)$ converge, and therefore, $e(t)$ will converge. To facilitate the subsequent development, let the composite error vector be defined as $z(t) \triangleq [e_1^T(t) \ e_2^T(t)]^T$.

IV. CONTROLLER AND UPDATE LAW DESIGN

To facilitate the subsequent analysis, two subsystems are defined to indicate when the states are inside or outside the feedback region. When $x(t) \in \mathcal{F}$, an exponentially stable observer can be designed using various approaches (e.g., observers such as [36], [38], and [39] could be used). The subsequent development is based on an observer update law designed as¹

$$\dot{\hat{x}}(t) = f(\hat{x}(t), t) + v(t) + v_r(t) \quad (5)$$

where $v_r(t) \in \mathbb{R}^n$ is a high-frequency sliding-mode term designed as²

$$v_r(t) = k_2 e_2(t) + \bar{d} \text{sgn}(e_2(t)) \quad (6)$$

where $k_2 \in \mathbb{R}^{n \times n}$ is a constant, positive definite gain matrix. When $x(t) \in \mathcal{F}^c$, the state estimate is updated by a predictor designed as

$$\dot{\hat{x}}(t) = f(\hat{x}(t), t) + v(t). \quad (7)$$

Since the state is required to transition between \mathcal{F} and \mathcal{F}^c , a switched systems analysis is used to investigate the stability of the overall switched system. To facilitate this analysis, the error systems for $e_1(t)$ and $e_2(t)$ are expressed as

$$\dot{e}_1(t) = f_{1p}(\bar{x}_d(t), \hat{x}(t), t) \quad (8)$$

$$\dot{e}_2(t) = f_{2p}(x(t), \hat{x}(t), t) \quad (9)$$

¹Once $x(t) \in \mathcal{F}$, a simple reset scheme (i.e., setting $\hat{x}(t) = x(t)$) could be used. The reset scheme would eliminate the subsequently developed minimum dwell time for which $x(t)$ is required to remain in the feedback region \mathcal{F} . However, the subsequent development is based on the continued use of the observer to illustrate a more general stability condition for systems that require an observer or $\dot{\hat{x}}(t) \in \mathcal{L}_\infty \forall t$.

²In cases where a piecewise-continuous controller is required, the robustifying term in (5) may be designed as $v_r(t) = k_2 e_2 + \frac{\bar{d}^2}{\epsilon} e_2$, where $\epsilon \in \mathbb{R}_{>0}$ is a design parameter.

where $f_{1p}, f_{2p} : \mathbb{R}^n \times \mathbb{R}^n \times \mathbb{R}_{\geq 0} \rightarrow \mathbb{R}^n$, $p \in \{a, u\}$, a is an index for subsystems with available feedback, and u is an index for subsystems when feedback is unavailable. Based on (8) and the subsequent stability analysis, the controller is designed as

$$v(t) = \begin{cases} \dot{\bar{x}}_d(t) - f(\hat{x}(t), t) - k_1 e_1(t) - v_r(t), & p = a \\ \dot{\bar{x}}_d(t) - f(\hat{x}(t), t) - k_1 e_1(t), & p = u \end{cases} \quad (10)$$

where $\dot{\bar{x}}_d(t) \in \mathbb{R}^n$, and $k_1 \in \mathbb{R}^{n \times n}$ is a constant, positive definite gain matrix. By taking the time derivative of (3) and substituting (5), (7), and (10) into the resulting expression, (8) can be expressed as

$$\dot{e}_1(t) = -k_1 e_1(t) \quad \forall p. \quad (11)$$

After taking the time derivative of (4) and substituting (1), (5), and (7) into the resulting expression, the family of systems in (9) can be expressed as

$$\dot{e}_2(t) = \begin{cases} f(x(t), t) - f(\hat{x}(t), t) + d(t) & p = a \\ -\bar{d} \text{sgn}(e_2(t)) - k_2 e_2(t) & p = a \\ f(x(t), t) - f(\hat{x}(t), t) + d(t) & p = u \end{cases} \quad (12)$$

V. SWITCHED SYSTEM ANALYSIS

To further facilitate the analysis for the switched system, let $t_i^a \in \mathbb{R}_{\geq 0}$ denote the time of the i th instance when $x(t)$ transitions from \mathcal{F}^c to \mathcal{F} , and $t_i^u \in \mathbb{R}_{>0}$ denote the time of the i th instance when $x(t)$ transitions from \mathcal{F} to \mathcal{F}^c , for $i \in \mathbb{N}$. The dwell time in the i th activation of the subsystems a and u is defined as $\Delta t_i^a \triangleq t_i^u - t_i^a \in \mathbb{R}_{>0}$ and $\Delta t_i^u \triangleq t_{i+1}^a - t_i^u \in \mathbb{R}_{>0}$, respectively. By Assumption 2 subsystem a is activated when $t = 0$, and consequently $t_i^u > t_i^a \forall i \in \mathbb{N}$.

Assumption 2: The system is initialized in a feedback region (i.e., $x(0) \in \mathcal{F}$).

To analyze the switched system, a common Lyapunov-like function is designed as

$$V_\sigma(z(t)) = V_1(e_1(t)) + V_2(e_2(t)) \quad (13)$$

where the candidate Lyapunov functions for the tracking error and the estimation error are selected, respectively, as

$$V_1(e_1(t)) = \frac{1}{2} e_1^T(t) e_1(t) \quad (14)$$

$$V_2(e_2(t)) = \frac{1}{2} e_2^T(t) e_2(t). \quad (15)$$

The common Lyapunov-like function $V_\sigma(z(t))$ globally exponentially converges when $x(t) \in \mathcal{F}$ and exhibits an exponential growth when $x(t) \in \mathcal{F}^c$. Hence, a desired maximum bound V_M and a minimum threshold V_T on $V_\sigma(z(t))$ may be imposed such that $V_\sigma(z(t)) \leq V_M$ and $V_\sigma(z(t_i^u)) \leq V_T$. A representative illustration for the evolution of $V_\sigma(z(t))$ is shown in Fig. 1. A lower threshold V_T enforces the convergence of $\|z(t)\|$ to an arbitrary small value. When implementing a high-frequency controller, V_T may be selected arbitrarily close to zero. However, the closer V_T is selected to zero, the longer $x(t)$ is required to remain in \mathcal{F} , and therefore, the selection of V_T is dependent on the individual application tolerance. When a high-gain controller (e.g., $v_r(t) = k_2 e_2(t) + \frac{\bar{d}^2}{\epsilon} e_2(t)$) is implemented, V_T should be selected such that $V_T \geq \epsilon$, where ϵ is a design parameter.

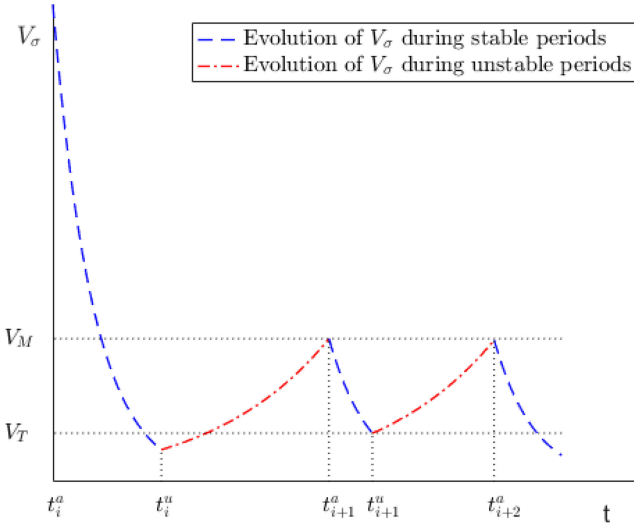


Fig. 1. Representative illustration for the evolution of V_σ during the interval $[t_i^a, t_{i+2}^a]$.

Theorem 1: The composite error system trajectories of the switched system generated by the family of subsystems described by (11), (12), and a piecewise constant, right continuous switching signal $\sigma : [0, \infty) \rightarrow p \in \{a, u\}$ are globally uniformly ultimately bounded provided the switching signal satisfies the minimum feedback availability dwell time condition

$$\Delta t_i^a \geq \frac{-1}{\lambda_s} \ln \left(\min \left(\frac{V_T}{V_\sigma(z(t_i^a))}, 1 \right) \right) \quad (16)$$

and the maximum loss of feedback dwell time condition

$$\Delta t_i^u \leq \frac{1}{\lambda_u} \ln \left(\frac{V_M + \frac{\bar{d}^2}{2\lambda_u}}{V_\sigma(z(t_i^u)) + \frac{\bar{d}^2}{2\lambda_u}} \right) \quad (17)$$

where λ_s and λ_u are subsequently defined known positive constants.

Proof: By taking the time derivative of (14) and substituting for (11) yields

$$\dot{V}_1(e_1(t)) \leq -2k_1 V_1(e_1(t)) \quad \forall t \quad (18)$$

where k_1 is the minimum eigenvalue of k_1 . By using (12), the time derivative of (15) can be expressed as

$$\dot{V}_2(e_2(t)) \leq \begin{cases} -2(k_2 - c)V_2(e_2(t)), & t \in [t_i^a, t_i^u) \\ \lambda_u V_2(e_2(t)) + \frac{1}{2}\bar{d}^2, & t \in [t_i^u, t_{i+1}^a) \end{cases} \quad (19)$$

where $c \in \mathbb{R}_{>0}$ is a Lipschitz constant, $k_2 > c \in \mathbb{R}$ is the minimum eigenvalue of k_2 , and $\lambda_u \triangleq 2c + 1 \in \mathbb{R}_{>0}$.

From (18) and (19), the time derivative of the common Lyapunov-like function can be expressed as

$$\dot{V}_\sigma(z(t)) \leq \begin{cases} -\lambda_s V_\sigma(z(t)), & t \in [t_i^a, t_i^u) \\ \lambda_u V_\sigma(z(t)) + \frac{1}{2}\bar{d}^2, & t \in [t_i^u, t_{i+1}^a) \end{cases} \quad \forall i \in \mathbb{N} \quad (20)$$

where $\lambda_s = 2\min(k_1, (k_2 - c)) \in \mathbb{R}_{>0}$. The solutions to (20) for the two subsystems are

$$V_\sigma(z(t)) \leq V_\sigma(z(t_i^a))e^{-\lambda_s(t-t_i^a)}, \quad t \in [t_i^a, t_i^u) \quad (21)$$

$$V_\sigma(z(t)) \leq V_\sigma(z(t_i^u))e^{\lambda_u(t-t_i^u)} - \frac{\bar{d}^2}{2\lambda_u} \left(1 - e^{\lambda_u(t-t_i^u)} \right), \quad t \in [t_i^u, t_{i+1}^a). \quad (22)$$

The inequality in (21) indicates that $\|z(t)\| \leq \|z(t_i^a)\| e^{-\frac{1}{2}\lambda_s(t-t_i^a)}$, $t \in [t_i^a, t_i^u)$. The minimum threshold V_T is selected to enforce the convergence of $\|z(t)\|$ to the desired threshold before allowing $x(t)$ to transition into \mathcal{F}^c . This condition can be expressed as $V_\sigma(z(t_i^a))e^{-\lambda_s \Delta t_i^a} \leq V_T$, and therefore, the condition in (16) is obtained after algebraic manipulation. If $\frac{V_T}{V_\sigma(z(t_i^a))} > 1$, the value of $V_\sigma(z(t_i^a))$ is already below the threshold and thus, no minimum dwell time is required for the subsystem.

When $t \in [t_i^u, t_{i+1}^a)$, the inequality in (22) indicates that $\|z\| \leq \sqrt{\|z(t_i^u)\|^2 e^{2\lambda_u(t-t_i^u)} - \frac{\bar{d}^2}{2\lambda_u}(1 - e^{2\lambda_u(t-t_i^u)})}$, and hence, the maximum bound V_M is selected to limit the growth of errors, where $V_M > V_T$. The maximum dwell time condition for each of the i th unstable periods is expressed as $V_\sigma(z(t_i^u))e^{\lambda_u \Delta t_i^u} - \frac{\bar{d}^2}{2\lambda_u}(1 - e^{\lambda_u \Delta t_i^u}) \leq V_M$, and therefore, the condition in (17) can be obtained.

Therefore, the composite error system trajectories generated by (11) and (12) are globally uniformly ultimately bounded as depicted in Fig. 1. ■

VI. SWITCHING TRAJECTORY DESIGN

Since x_d lies outside the feedback region, i.e., $x_d \subset \mathcal{F}^c \forall t$, and cannot be followed for all time, the switching trajectory $\bar{x}_d(t)$ is designed to enable $x(t)$ to follow x_d to the extent possible given the dwell time conditions in (16) and (17). A design challenge for $\bar{x}_d(t)$ is to ensure $x(t)$ reenters \mathcal{F} to satisfy the sufficient condition in (17). While $x(t)$ transitions through \mathcal{F}^c , $e(t)$ may grow as indicated by (22), and this growth must be accounted for when designing $\bar{x}_d(t)$. To facilitate the development of the switching trajectory $\bar{x}_d(t)$, $x_b(t) \in \mathbb{R}^n$ is defined as the closest orthogonal projection of $\bar{x}_d(t)$ on the boundary of \mathcal{F} .

When the maximum dwell time condition is reached, $\|e(t)\| \leq 2\sqrt{V_M}$. This bound implies that there exists a set $\mathcal{B} = \{y \in \mathbb{R}^n \mid \|y - \bar{x}_d(t)\| \leq 2\sqrt{V_M}\}$ such that $x(t) \in \mathcal{B} \forall t$. Therefore, the switching trajectory must penetrate a sufficient distance into \mathcal{F} to compensate for the error accumulation. The distance to compensate for error growth motivates the design of a cushion that ensures the reentry of the actual states when the maximum dwell time is reached. To compensate for the potential accumulation of error, $\bar{x}_d(t)$ must penetrate a sufficient distance into \mathcal{F} , motivating the design of a cushion state $x_\epsilon(t) \in \mathbb{R}^n$ as

$$x_\epsilon(t) \triangleq x_b(t) + \Phi(t)$$

where $\Phi(t) \in \mathbb{R}^n$, such that $\|\Phi(t)\| \geq 2\sqrt{V_M}$ and there exists a compact set $\mathcal{A} = \{y \in \mathbb{R}^n \mid \|y - x_\epsilon(t)\| \leq \|\Phi(t)\|\}$ such that \mathcal{A} is less than or equal to the inscribed ball of \mathcal{F} in \mathbb{R}^n . Therefore, the requirement of $x(t) \in \mathcal{B} \subseteq \mathcal{A} \subseteq \mathcal{F}$ can be satisfied if $x_\sigma(t)$ coincides with $x_\epsilon(t)$ when the maximum dwell time is reached.

A. Design Example

An example switching trajectory $\bar{x}_d(t)$ can be developed utilizing a smootherstep function described in [40] to transition smoothly between x_d and $x_\epsilon(t)$ while meeting the dwell time conditions (see Remark 1). The smootherstep function is defined in [40] as

$$S(\rho) = 6\rho^5 - 15\rho^4 + 10\rho^3 \quad (23)$$

where $\rho \in [0, 1]$ is the input parameter. Given the transition function in (23), the switching trajectory is designed as

$$\bar{x}_d(t) \triangleq \begin{cases} H\left(S(\rho_i^a), x_b(t), x_\epsilon(t)\right), & t_i^a \leq t < t_i^u \\ H\left(S(\rho_i^{u1}), g(x_d, t), x_b(t)\right), & t_i^u \leq t < t_i^{u1} \\ H\left(S(\rho_i^{u2}), g(x_d, t), g(x_d, t)\right), & t_i^{u1} \leq t < t_i^{u2} \\ H\left(S(\rho_i^{u3}), x_\epsilon(t), g(x_d, t)\right), & t_i^{u2} \leq t < t_i^{u3} \end{cases} \quad (24)$$

where $H(S(\cdot), q(t), r(t)) \triangleq S(\cdot)q(t) + [1 - S(\cdot)]r(t)$ for $q(t), r(t) \in \mathbb{R}^n, g: x_d \times \mathbb{R} \rightarrow \mathbb{R}^n$ gives the desired state on x_d at time t , $\rho_i^a, \rho_i^{u1}, \rho_i^{u2}$, and ρ_i^{u3} are designed as $\rho_i^a \triangleq \frac{t - t_i^a}{\Delta t_i^a}$ and $\rho_i^{u,j+1} \triangleq \frac{t - (t_i^u + \sum_{k=0}^j p_k \Delta t_i^u)}{p_{j+1} \Delta t_i^u}$, $j \in \{0, 1, 2\}$, the weights used to partition the maximum dwell time are denoted by $p_k \in [0, 1]$, and the corresponding partitions are denoted by $t_i^{u,j+1}$. The final partition t_i^{u3} coincides with t_{i+1}^a . To avoid singularity in ρ_i^a and to ensure a smooth and continuous switching trajectory, Δt_i^a must be arbitrarily lower bounded above zero (see Remark 2).

Remark 1: The switching trajectory is designed to compensate for the worst-case scenario where it must penetrate the entirety of the cushion to ensure $x(t)$ enters \mathcal{F} . However, if $x(t)$ is able to reach \mathcal{F} before the dwell time condition is reached, the agent may remain stationary for the entirety of the minimum dwell time. Other trajectories satisfying the dwell time conditions in Theorem 1 may also be implemented, such as the work in [37].

Remark 2: Lower bounding Δt_i^a by an arbitrary value $\alpha \in \mathbb{R}_{>0}$ does not violate Theorem 1 since the system is allowed to remain in the feedback region longer than the minimum dwell time, implying that $\Delta t_i^a \leq \alpha \leq (t - t_i^a)$ holds. Other trajectory designs may not require Δt_i^a to be lower bounded.

VII. SIMULATION

A simulation is performed to illustrate the performance of the controller, given the intermittent loss-of-state feedback. Based on the system model given in (1), $f(x(t), t)$ is selected as $f(x(t), t) = Ax$ where $A = 0.5I_3$, and $d(t)$ is drawn from a uniform distribution between $[0, 0.06]$ m/s. The initial states and estimates are selected as $x(0) = [0.1 \text{ m } 0.2 \text{ m } 0 \text{ rad}]$ and $\hat{x}(0) = [0.2 \text{ m } 0.3 \text{ m } \frac{\pi}{6} \text{ rad}]$. The observer and the controller gains were selected as $k_1 = 3I_3$ and $k_2 = 3I_3$, respectively. The desired upper bound and lower threshold for the composite error $\|z(t)\|$ are selected as 0.9 and 0.02 m, respectively. Based on the desired error bound and threshold, the

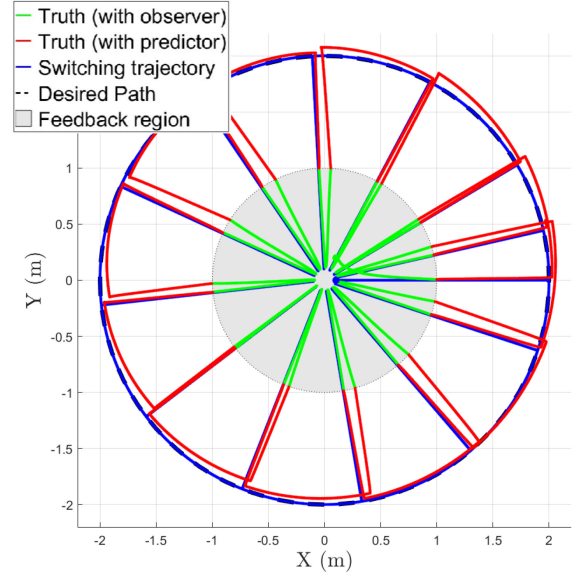


Fig. 2. Simulation result for 30 s. Both system state $x(t)$ and switching trajectory $\bar{x}_d(t)$ are initialized in the feedback region (gray). During the minimum dwell time, $x(t)$ converges to $\bar{x}_d(t)$ exponentially with the observer activated. When $x(t)$ transitions into the feedback-denied region (white), the predictor is activated, and $x(t)$ gradually diverges from $\bar{x}_d(t)$ due to disturbances. Before the maximum dwell time is reached, $x(t)$ reenters the feedback region and the observer is reactivated. Hence, $x(t)$ is able to converge to $\bar{x}_d(t)$.

Lyapunov function bound and threshold are determined as $V_M = 0.2025$ and $V_T = 1 \times 10^{-4}$.

The desired path x_d is selected as a circular trajectory with a radius of 2 m centered at the origin. The boundary of the feedback region is selected as a circle with a 1-m radius about the origin. The switching trajectory $\bar{x}_d(t)$ were designed as described in Section VI and follows x_d at $\frac{\pi}{5}$ rad/s, where the partition weights are selected as $p_0 = 0, p_1 = 0.3, p_2 = 0.4$, and $p_3 = 0.3$.

Fig. 2 depicts the agent's planar trajectory and shows that when the agent was inside the region with state feedback, both the estimation and tracking errors, $\|e_1(t)\|$ and $\|e_2(t)\|$, exponentially converged. When the agent was outside the feedback region, the tracking error converged while the predictor error exhibited exponential divergence.

The average maximum and minimum dwell times between switches are 2.16 and 0.26 s, respectively. Based on the simulation result, the system is allowed to remain 8.23 times longer outside the feedback region than inside on average. Furthermore, 40% of the maximum dwell time is dedicated to following the desired path, which translates to 36% of the combined duration of the maximum and minimum dwell times per cycle.

In Fig. 3, the composite error $\|z(t)\|$ is shown. Fig. 3 indicates that $\|z(t)\|$ remained below 0.9 m for all time and less than or equal to 0.02 (indicated by the black dashed line) by the end of each stable period, which demonstrates the robustness of the presented control design under the dwell time condition constraints and disturbances. Since an exact model of the system was used in this simulation, the resulting tracking error is bounded well-below the maximum bound, and hence emphasizing the conservative nature of the Lyapunov analysis method.

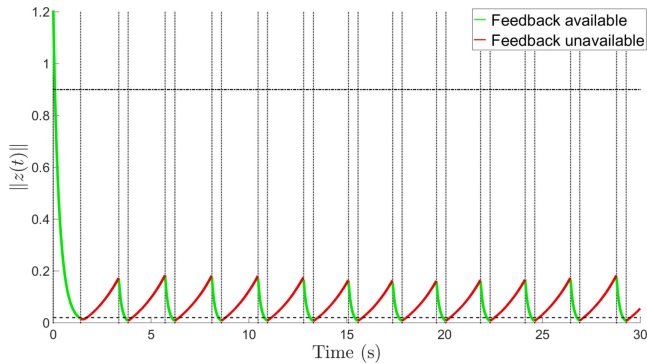


Fig. 3. Evolution of $\|z(t)\|$. The top dashed line denotes V_M and the bottom dashed line denotes V_T .

VIII. EXPERIMENTS

In this section, an experiment is performed to verify the theoretical results where a single integrator dynamic is used instead of the exact system model. The overall goal of the experiment is to represent a scenario where an unmanned air vehicle is tasked with following a path where feedback is not available (e.g., inside an urban canyon). Specifically, the objective is to demonstrate the boundedness of the tracking error $e(t)$ through multiple cycles of switching between the feedback-available and unavailable regions based on the dwell time constraints established in Section V. A Parrot Bebop 2.0 quadcopter is used as the unmanned air vehicle. The quadcopter is equipped with a 3-axis gyroscope, a 3-axis accelerometer, an ultrasound sensor, and an optical-flow sensor. The onboard sensors provide an estimate of the linear and angular velocities of the quadcopter at 5 Hz. To control the quadcopter, the *bebop_autonomy* package developed by [41] is utilized to send velocity commands generated from an off board computer running Robotic Operating System (ROS) Kinetic in Ubuntu 16.04. The communication link between the computer and the quadcopter is established through a WiFi channel at 5 GHz.

A NaturalPoint, Inc. OptiTrack motion capture system is used to simulate a feedback signal and record the ground truth pose of the quadcopter at a rate of 120 Hz. While the quadcopter is inside the feedback region, pose information from the motion capture system is directly used as feedback in the controller and update laws designed in Section IV. When the quadcopter operated outside the feedback region, the pose feedback is discarded. During these times, the onboard velocity measurements are used to feedforward the state estimate. Although the OptiTrack system continue to record the pose of the quadcopter, the pose information is only used as the ground truth for illustration purposes.

Utilizing the motion capture system, a circular region of available feedback is centered at the origin of the Euclidean world frame with a radius of 1 m. Since torque level control authority is not available, single integrator dynamics $\dot{q}(t) = u(t) + d(t)$ are assumed for the quadcopter where $q(t) = [x(t) \ y(t) \ z(t) \ \alpha(t)]^T$, and $x(t), y(t), z(t), \alpha(t) \in \mathbb{R}$ are the three-dimensional (3-D) Euclidean coordinates and yaw rotation of the quadcopter with respect to the inertial frame. The

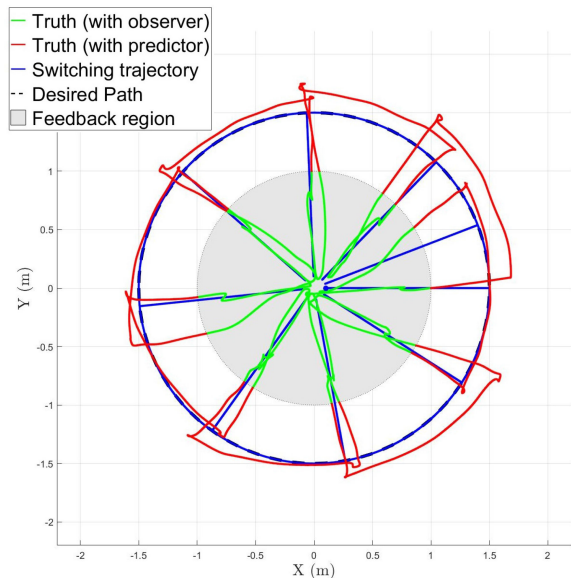


Fig. 4. Actual and switching trajectory over 185 seconds.

disturbance is assumed to be upper bounded as $\bar{d} = 0.035$. To compensate for the disturbance, a high-gain robust controller is implemented to ensure a continuous control command. The controller and update law gains are selected as $k_1 = 0.4I_4$, $k_2 = 0.6I_4$, and $\epsilon = 0.1$. To regulate and match the actual velocity output to the control command, a low-level PID controller is implemented.

The desired upper bound and lower threshold on $\|z(t)\|$ are selected as 0.9 and 0.14 m, respectively. Since single integrator dynamics are assumed for the quadcopter dynamic, a less conservative minimum dwell time condition can be derived (details are given in the Appendix). The desired path is defined as a circular path centered at the origin with a radius of 1.5 m. In this experiment, the desired circular path starts at $[1.5 \ 0]^T$ m and revolves counterclockwise. Following the design method outlined in Section VI, a switching trajectory is designed to follow x_d with an angular velocity of $\frac{\pi}{15}$ rad/s. To prevent the quadcopter from drifting out of the feedback region prematurely, an intermediate trajectory is designed to be $x_{\text{int}}(t) = 0.7x_b(t)$ to replace $x_b(t)$ in (24) as a safety measure. The partitions for the maximum dwell time are selected as $p_0 = 0$, $p_1 = 0.4$, $p_2 = 0.2$, and $p_3 = 0.4$.

Initially, the quadcopter is launched inside \mathcal{F} along with the switching trajectory, which transitions between \mathcal{F} and x_d over the prescribed time span. The experimental results demonstrate that the quadcopter is capable of intermittently leaving \mathcal{F} to follow x_d for some period of time and then, return to \mathcal{F} consistently. The supplementary video accompanying this paper, available for download at <http://ieeexplore.ieee.org>, gives a recording of the experiment with the motion of the quadcopter and the switching trajectory projected on the floor. The overall path-following plot, including the desired path, switching trajectory, and actual states, is shown in Fig. 4, where a total of eight cycles of leaving and reentering \mathcal{F} occurred. As shown in Fig. 4, the tracking performance outside of the feedback-available region is heavily affected by aerodynamic disturbances. Specifically, the right half

TABLE I
MINIMUM AND MAXIMUM DWELL TIMES

Cycle	Max. D. T. (s)	Min. D. T. (s)
0	-	3.50
1	19.12	4.55
2	19.38	4.09
3	19.25	3.20
4	19.72	3.34
5	20.21	1.67
6	19.08	2.55
7	19.65	3.73
8	22.35	3.16
Avg	19.85	3.31

TABLE II
MAXIMUM DWELL TIME PARTITIONS

Cycle	Maximum dwell times (s)		
	Part. 1 (40%)	Part. 2 (20%)	Part. 3 (40%)
1	7.65	3.82	7.65
2	7.75	3.88	7.75
3	7.70	3.85	7.70
4	7.89	3.94	7.89
5	8.08	4.04	8.08
6	7.63	3.82	7.63
7	7.86	3.93	7.86
8	8.94	4.47	8.94

of the trajectory exhibits a worse tracking performance likely due to airflow in the room, causing the vehicle to drift away from its estimate. Table I indicates the maximum and minimum dwell times for each cycle. On average, the quadcopter was allowed to reside approximately six times longer in \mathcal{F}^c than \mathcal{F} , and 20% of which is dedicated to following x_d . Specifically, the quadcopter is allowed 19.85 s in \mathcal{F}^c and is required to remain in \mathcal{F} for 3.31 s on average. Based on the partition weights of the maximum dwell time, Table II describes the partitions and the duration for each partition. During partition 1, $\bar{x}_d(t)$ transitions from $x_b(t)$ to x_d where the partition weight was set to 50%. The relatively large partition allots more time in transition to yield a slower velocity profile, which produces less overshoot in the tracking performance. The distance between x_d and \mathcal{F} is also a major factor in distributing partition weights in the sense that the closer x_d is to \mathcal{F} , the less time is required for transition and more time can be allocated to follow x_d .

To illustrate the stability of the control scheme, the Euclidean norm of the estimate tracking error $e_1(t)$ and the estimation error $e_2(t)$ are displayed in Figs. 5 and 6. The estimate tracking error exponentially converges, reflecting the analysis in (18). The estimation error exhibits growth when $x(t) \in \mathcal{F}^c$. For a better illustration, the norm of the composite and actual tracking error are shown in Figs. 7 and 8, respectively, where the dwell time duration is indicated by vertical dash-dot lines and the upper bound and lower threshold on the actual tracking error are indicated by horizontal dashed lines. Over the eight cycles, $\|z(t)\|$ is upper bounded by 0.9 m at all times, and converges to below 0.14 m within the minimum dwell time when $x(t) \in \mathcal{F}$. The plots also indicate that $x(t)$ is able to return to \mathcal{F} within the maximum dwell times. This can be verified by the activation of the observer before the maximum dwell time is reached

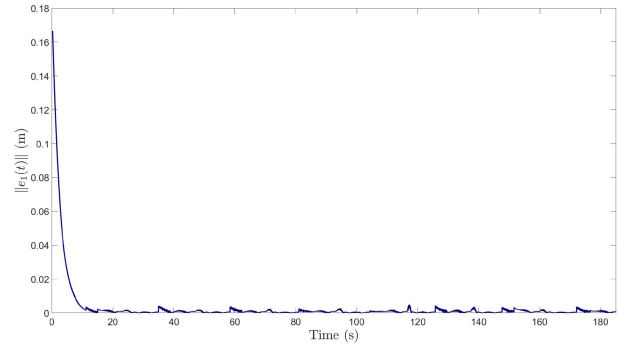


Fig. 5. Estimate tracking error $\|e_1(t)\|$. As indicated by the analysis, the estimate tracking error exhibits exponential stability regardless of feedback availability.

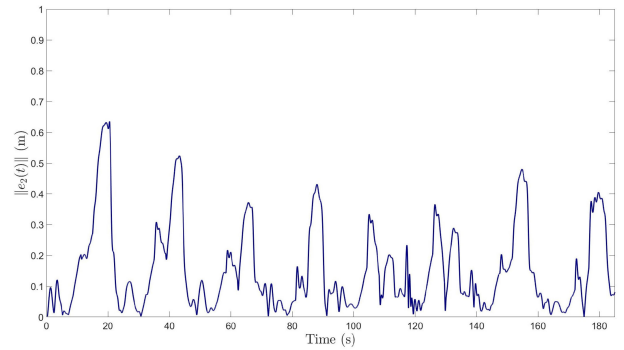


Fig. 6. Estimation error $\|e_2(t)\|$. As indicated by the analysis, the estimation error converges when $x(t) \in \mathcal{F}$ and diverges when $x(t) \in \mathcal{F}^c$.

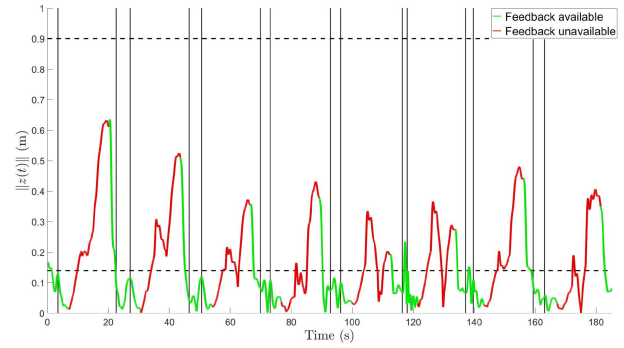


Fig. 7. Evolution of $\|z(t)\|$. The dash-dot (vertical) lines indicate the switching interface of minimum and maximum dwell times, and the dashed (horizontal) lines indicate the prescribed upper bound and lower threshold.

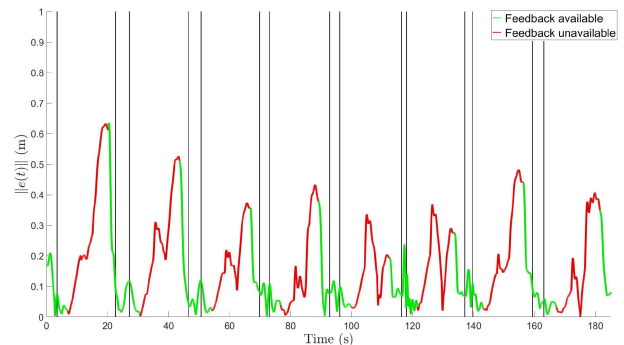


Fig. 8. Actual tracking error $\|e(t)\|$. The dash-dot lines indicate the switching interface of minimum and maximum dwell times.

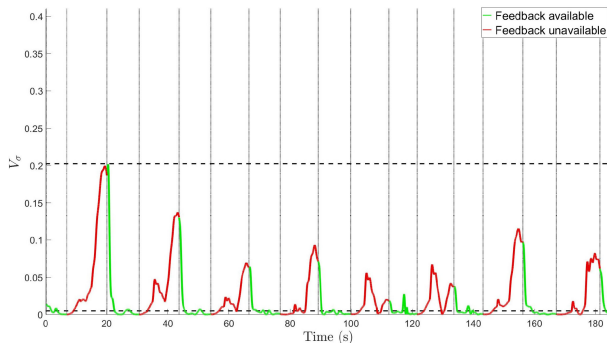


Fig. 9. Evolution of $V_\sigma(t)$. The dotted (vertical) lines indicate the time instants when the quadcopter crossed the feedback region boundary. The dashed (horizontal) lines indicate the prescribed V_M and V_T for V_σ .

for every cycle. In Fig. 9, the evolution of V_σ is shown along with the calculated V_M and V_T as indicated by the horizontal dashed lines. As expected, the Lyapunov-like function V_σ is upper bounded below V_M for all times and converges below V_T within the minimum dwell times. Based on Figs. 8 and 9, the controller and update laws developed in Section IV demonstrate robustness towards disturbances and a simple assumed dynamic model. Hence, the trajectory design scheme provided in Section VI is able to generate a switching signal $\sigma(t)$ that satisfied the dwell time conditions developed in Section V and, therefore, verifying the claim in Theorem 1.

IX. CONCLUSION

In this paper, a novel method that utilizes a switched systems approach to ensure path-following stability under intermittent state feedback was presented. The presented method relieved the requirement of state feedback at all times. State estimates were used in the tracking control to compensate for the intermittence of state feedback. A Lyapunov-based switched systems analysis was used to develop maximum and minimum dwell time conditions to guarantee stability of the overall system. The dwell time conditions allowed the desired path to be completely outside the feedback region, and a switching trajectory was designed to bring the states back into the feedback region before the error growth exceeded a defined threshold. The candidate switching trajectory switched between the desired path and the feedback region using smootherstep transition functions. A simulation and an experiment were performed to illustrate the robustness of the control and trajectory design. Less conservative analysis methods were motivated for future work as a means to reduce the conservative nature of the dwell time conditions in this paper. In addition, future research will focus on the development of an approximate optimal control approach using adaptive dynamic programming concepts to yield approximately optimal results. Further efforts will also examine cases where the feedback region is time varying or unknown.

APPENDIX

When using single integrator dynamics $\dot{x}(t) = u + d(t)$, the resulting estimation error dynamics for the unstable subsystem is $\|\dot{e}_2(t)\| \leq \bar{d}$, and the corresponding Lyapunov-like

function derivative is $\dot{V}_\sigma(t) \leq \bar{d}\|e_2(t)\|$. By solving the ordinary differential equation for $\dot{e}_2(t)$, the estimation error $e_2(t)$ exhibits a linear growth that can be bounded as $e_2(t) \leq e_2(t_i^u) + \bar{d}(t - t_i^u)$. After substituting in the linear bound on $e_2(t)$, it follows that $\dot{V}_\sigma(t) \leq \bar{d}\|e_2(t_i^u)\| + \bar{d}^2(t - t_i^u)$, and solving the ordinary differential equation yields $V_\sigma(t) \leq \frac{1}{2}\bar{d}^2(t - t_i^u)^2 + \bar{d}\|e_2(t_i^u)\|(t - t_i^u) + V_\sigma(z(t_i^u))$. After imposing $V_\sigma(t) \leq V_M$ as the upper bound constraint, the maximum dwell time can be derived by solving the quadratic equation and taking the positive root as

$$\Delta t_i^u \leq \frac{\left(\sqrt{\|e_2(t_i^u)\|^2 - 2(V_\sigma(z(t_i^u)) - V_M)} - \|e_2(t_i^u)\|\right)}{\bar{d}}.$$

ACKNOWLEDGMENT

Any opinions, findings and conclusions, or recommendations expressed in this material are those of the author(s) and do not necessarily reflect the views of the sponsoring agency.

REFERENCES

- [1] N. Gans, S. Hutchinson, and P. Corke, "Performance tests for visual servo control systems, with application to partitioned approaches to visual servo control," *Int. J. Rob. Res.*, vol. 22, no. 10, pp. 955–981, 2003.
- [2] S. Hutchinson, G. Hager, and P. Corke, "A tutorial on visual servo control," *IEEE Trans. Robot. Autom.*, vol. 12, no. 5, pp. 651–670, Oct. 1996.
- [3] N. Gans, G. Hu, K. Nagarajan, and W. E. Dixon, "Keeping multiple moving targets in the field of view of a mobile camera," *IEEE Trans. Robot. Autom.*, vol. 27, no. 4, pp. 822–828, Aug. 2011.
- [4] N. Gans, G. Hu, J. Shen, Y. Zhang, and W. E. Dixon, "Adaptive visual servo control to simultaneously stabilize image and pose error," *Mechatronics*, vol. 22, no. 4, pp. 410–422, 2012.
- [5] G. Hu, N. Gans, and W. E. Dixon, "Quaternion-based visual servo control in the presence of camera calibration error," *Int. J. Robust Nonlinear Control*, vol. 20, no. 5, pp. 489–503, 2010.
- [6] G. Hu, N. Gans, N. Fitz-Coy, and W. E. Dixon, "Adaptive homography-based visual servo tracking control via a quaternion formulation," *IEEE Trans. Control Syst. Technol.*, vol. 18, no. 1, pp. 128–135, Jan. 2010.
- [7] G. Hu *et al.*, "Homography-based visual servo control with imperfect camera calibration," *IEEE Trans. Autom. Control*, vol. 54, no. 6, pp. 1318–1324, Jun. 2009.
- [8] J. Chen, D. M. Dawson, W. E. Dixon, and V. Chitrakaran, "Navigation function-based visual servo control," *Automatica*, vol. 43, pp. 1165–1177, 2007.
- [9] J. Chen, D. M. Dawson, W. E. Dixon, and A. Behal, "Adaptive homography-based visual servo tracking for fixed and camera-in-hand configurations," *IEEE Trans. Control Syst. Technol.*, vol. 13, no. 5, pp. 814–825, Sep. 2005.
- [10] G. Palmieri, M. Palpacelli, M. Battistelli, and M. Callegari, "A comparison between position-based and image-based dynamic visual servoings in the control of a translating parallel manipulator," *J. Robot.*, vol. 2012, 2012, Art. no. 103954.
- [11] N. Gans and S. Hutchinson, "Stable visual servoing through hybrid switched-system control," *IEEE Trans. Robot.*, vol. 23, no. 3, pp. 530–540, Jun. 2007.
- [12] G. Chesi and A. Vicino, "Visual servoing for large camera displacements," *IEEE Trans. Robot. Autom.*, vol. 20, no. 4, pp. 724–735, Aug. 2004.
- [13] N. R. Gans and S. A. Hutchinson, "A stable vision-based control scheme for nonholonomic vehicles to keep a landmark in the field of view," in *Proc. IEEE Int. Conf. Robot. Autom.*, Roma, Italy, 2007, pp. 2196–2201.
- [14] G. L. Mariottini, G. Oriolo, and D. Prattichizzo, "Image-based visual servoing for nonholonomic mobile robots using epipolar geometry," *IEEE Trans. Robot.*, vol. 23, no. 1, pp. 87–100, Feb. 2007.
- [15] G. Lopez-Nicolas, N. R. Gans, S. Bhattacharya, C. Sagues, J. J. Guerrero, and S. Hutchinson, "Homography-based control scheme for mobile robots with nonholonomic and field-of-view constraints," *IEEE Trans. Syst., Man, Cybern.*, vol. 40, no. 4, pp. 1115–1127, Aug. 2010.
- [16] G. Conte, G. de Capua, and D. Scaradozzi, "Designing the NGC system of a small ASV for tracking underwater targets," *Robot. Auton. Syst.*, vol. 76, no. C, pp. 46–57, Feb. 2016.

- [17] K. Tanakitkorn, P. A. Wilson, S. R. Turnock, and A. B. Phillips, "Sliding mode heading control of an overactuated, hover-capable autonomous underwater vehicle with experimental verification," *J. Field Robot.*, vol. 35, no. 3, pp. 396–415, 2018.
- [18] L. Jianfang, Z. Hao, and G. Jingli, "A novel fast target tracking method for UAV aerial image," *Open Phys.*, vol. 15, Jun. 2017, Art. no. 46.
- [19] S. S. Mehta, G. Hu, A. P. Dani, and W. E. Dixon, "Multireference visual servo control of an unmanned ground vehicle," in *Proc. AIAA Guid. Navigat. Control Conf.*, Honolulu, Hawaii, Aug. 2008.
- [20] B. Jia and S. Liu, "Switched visual servo control of nonholonomic mobile robots with field-of-view constraints based on homography," *Control Theory Technol.*, vol. 13, no. 4, pp. 311–320, 2015.
- [21] G. Klein and D. Murray, "Parallel tracking and mapping for small AR workspaces," in *Proc. IEEE ACM Int. Symp. Mixed Augmented Reality*, 2007, pp. 225–234.
- [22] A. J. Davison, I. D. Reid, N. D. Molton, and O. Stasse, "MonoSLAM: Real-time single camera SLAM," *IEEE Trans. Pattern Anal. Mach. Intell.*, vol. 29, no. 6, pp. 1052–1067, Jun. 2007.
- [23] D. Cremers, "Direct methods for 3-D reconstruction and visual slam," in *Proc. IEEE IAPR Int. Conf. Mach. Vis. Appl.*, 2017, pp. 34–38.
- [24] B. Williams, M. Cummins, J. Neira, P. Newman, I. Reid, and J. Tardós, "A comparison of loop closing techniques in monocular SLAM," *Robot. Auton. Syst.*, vol. 57, no. 12, pp. 1188–1197, 2009.
- [25] C. Cadena *et al.*, "Past, present, and future of simultaneous localization and mapping: Towards the robust-perception age," *IEEE Trans. Robot.*, vol. 32, no. 6, pp. 1309–1332, Dec. 2016.
- [26] E. Garcia and P. J. Antsaklis, "Adaptive stabilization of model-based networked control systems," in *Proc. Amer. Control Conf.*, San Francisco, CA, USA, 2011, pp. 1094–1099.
- [27] S. S. Mehta, W. MacKunis, S. Subramanian, E. L. Pasiliao, and J. W. Curtis, "Stabilizing a nonlinear model-based networked control system with communication constraints," in *Proc. Amer. Control Conf.*, Washington, DC, USA, 2013, pp. 1570–1577.
- [28] E. Garcia and P. J. Antsaklis, "Model-based event-triggered control for systems with quantization and time-varying network delays," *IEEE Trans. Autom. Control*, vol. 58, no. 2, pp. 422–434, Feb. 2013.
- [29] M. J. McCourt, E. Garcia, and P. J. Antsaklis, "Model-based event-triggered control of nonlinear dissipative systems," in *Proc. Amer. Control Conf.*, Portland, OR, USA, 2014, pp. 5355–5360.
- [30] N. E. Leonard and A. Olshevsky, "Cooperative learning in multiagent systems from intermittent measurements," in *Proc. IEEE Conf. Decis. Control*, Florence, Italy, 2013, pp. 7492–7497.
- [31] J. Liang, Z. Wang, and X. Liu, "Distributed state estimation for discrete-time sensor networks with randomly varying nonlinearities and missing measurements," *IEEE Trans. Neural Netw.*, vol. 22, no. 3, pp. 486–496, Mar. 2011.
- [32] Y. Shi, H. Fang, and M. Yan, "Kalman filter-based adaptive control for networked systems with unknown parameters and randomly missing outputs," *Int. J. Robust Nonlinear Control*, vol. 19, no. 18, pp. 1976–1992, Dec. 2009.
- [33] D. Liberzon, *Switching in Systems and Control*. Basel, Switzerland: Birkhauser, 2003.
- [34] G. Zhai, B. Hu, K. Yasuda, and A. N. Michel, "Stability analysis of switched systems with stable and unstable subsystems: An average dwell time approach," *Int. J. Syst. Sci.*, vol. 32, no. 8, pp. 1055–1061, Nov. 2001.
- [35] M. A. Müller and D. Liberzon, "Input/output-to-state stability and state-norm estimators for switched nonlinear systems," *Automatica*, vol. 48, no. 9, pp. 2029–2039, 2012.
- [36] A. Parikh, T.-H. Cheng, H.-Y. Chen, and W. E. Dixon, "A switched systems framework for guaranteed convergence of image-based observers with intermittent measurements," *IEEE Trans. Robot.*, vol. 33, no. 2, pp. 266–280, Apr. 2017.
- [37] H.-Y. Chen, Z. I. Bell, R. Licitra, and W. E. Dixon, "Switched systems approach to vision-based tracking control of wheeled mobile robots," in *Proc. IEEE Conf. Decis. Control*, 2017, pp. 4902–4907.
- [38] A. Dani, N. Fischer, Z. Kan, and W. E. Dixon, "Globally exponentially stable observer for vision-based range estimation," *Mechatronics*, vol. 22, no. 4, Special Issue on Visual Servoing, pp. 381–389, 2012.
- [39] Z. I. Bell, H.-Y. Chen, A. Parikh, and W. E. Dixon, "Single scene and path reconstruction with a monocular camera using integral concurrent learning," in *Proc. IEEE Conf. Decis. Control*, 2017, pp. 3670–3675.
- [40] D. S. Ebert, *Texturing & Modeling: A Procedural Approach*. Burlington, MA, USA: Morgan Kaufmann, 2003.
- [41] bebop_Autonomy Library. Accessed: Mar. 20, 2018. [Online]. Available: <http://bebop-autonomy.readthedocs.io>



Hsi-Yuan (Steven) Chen received the Ph.D. degree in mechanical engineering from the Department of Mechanical and Aerospace Engineering, University of Florida, Gainesville, FL, USA, in 2018.

He is experienced in computer vision-based state estimation and Lyapunov-based control techniques for uncertain nonlinear systems. His main research interest includes the development of state-of-the-art control methods for autonomous vehicles.



Zachary Bell received the B.S. degree in mechanical engineering with a minor in electrical engineering and the M.S. degree in mechanical engineering in 2015 and 2017, respectively, from the University of Florida, Gainesville, FL, USA, where is currently working toward the Ph.D. degree in mechanical engineering under the supervision of Dr. Warren Dixon with the Nonlinear Controls and Robotics Group.

His research interests include Lyapunov-based estimation and control theory, visual estimation, simultaneous localization and mapping, and mechanical design.

Dr. Bell is the recipient of the Science, Mathematics, and Research for Transformation (SMART) Scholarship, an award sponsored by the Department of Defense, in 2018.



Patryk Deptula received the B.Sc. degree in mechanical engineering and a mathematics minor (Hons.), from Central Connecticut State University (CCSU), New Britain, CT, USA, in 2014, working on research related to hybrid propellant rocket engines. He is currently working toward the Ph.D. degree in mechanical engineering under the supervision of Dr. Warren Dixon, working on nonlinear controls and autonomy, with a focus on learning-based and adaptive control in a variety of applications.

After graduating, he worked as an Engineer with the Control and Diagnostic Systems (DSC) Group, Belcan Corporation, where he analyzed aircraft engine software. His research interests include, but are not limited to, multiagent systems, human-machine interaction, and robotics applied to a variety of fields.



Warren Dixon received the Ph.D. degree in electrical engineering from the Department of Electrical and Computer Engineering, Clemson University, Clemson, SC, USA, in 2000.

He worked as a Research Staff Member and Eugene P. Wigner Fellow at Oak Ridge National Laboratory (ORNL) till 2004, when he joined the University of Florida in the Mechanical and Aerospace Engineering Department, where he is an Ebaugh Professor. His main research interest includes the development and application of Lyapunov-based control techniques for uncertain nonlinear systems.

Dr. Dixon is the recipient of the 2009 and 2015 American Automatic Control Council (AACC) O. Hugo Schuck (Best Paper) Award, the 2013 Fred Ellersick Award for Best Overall MILCOM Paper, the 2011 American Society of Mechanical Engineers (ASME) Dynamics Systems and Control Division Outstanding Young Investigator Award, and the 2006 IEEE Robotics and Automation Society (RAS) Early Academic Career Award. He was awarded the Air Force Commander's Public Service Award (2016) for his contributions to the U.S. Air Force Science Advisory Board. He is currently or formerly an Associate Editor for the *ASME Journal of Journal of Dynamic Systems, Measurement and Control*, *Automatica*, *IEEE CONTROL SYSTEMS*, *IEEE TRANSACTIONS ON SYSTEMS MAN AND CYBERNETICS: PART B CYBERNETICS*, and the *International Journal of Robust and Nonlinear Control*. He is an ASME Fellow.